Ex Vivo Entrainment of the Isolated Mammalian Biological Clock Reveals Intrinsic Plasticity in Clock Gene Rhythm Dynamics

Authors:

Suil Kim[1] and Douglas G. McMahon*[1,2]

Author Affiliations:

[1]Vanderbilt Brain Institute, Vanderbilt University, Nashville, TN, USA

[2]Department of Biological Sciences, Vanderbilt University, Nashville, TN, USA

*Correspondence to: douglas.g.mcmahon@vanderbilt.edu

Abstract

The suprachiasmatic nucleus (SCN) in the brain, the central circadian clock, governs timekeeping under different lighting conditions throughout seasons. It remains elusive how circadian alignment with various light cycles is achieved by the SCN at the level of core clock gene rhythms. We instituted *ex vivo* long-term periodic optogenetic stimulation and bioluminescence recording on a timescale of weeks to study circadian entrainment of core clock gene PER2 rhythms in the isolated SCN. We show that a single early-night optogenetic stimulation elongates the PER2 falling phase, while a late-night stimulation contracts the rising phase, to induce delay and advance phase resetting. Phase resetting also resulted in subsequent persistent changes in clock period – with phase advances leading to period shortening, and phase delays resulting in lengthening. We demonstrate stable entrainment of the isolated clock to 22h and 25h stimulation cycles, which is achieved via repeated rising phase shortening and falling phase lengthening, respectively. When presented with optogenetic skeleton photoperiods (2 pulses/24h cycle) that simulate short-day or long-day photoperiods, isolated SCN entrained preferentially to the short-day photoperiod by phase-jumping, similar to circadian behavioral plasticity classically described in intact mice and files. Skeleton photoperiod entrainment is achieved via increasing the relative duration of the falling phase to the rising phase. Clock gene waveform changes are specific to entrainment as they do not persist following release into constant darkness. Our results reveal how core clock gene rhythms in the SCN encode different lighting conditions, and that key aspects of circadian behavioral plasticity reside within the SCN itself.

Introduction

Most organisms live in a rhythmic environment where daily environmental changes occur corresponding with solar time, and their endogenous 24-hour timing mechanism, or the circadian clock, enables adjustment of their physiology and behavior accordingly. In mammals, the central clock—the suprachiasmatic nucleus (SCN) of the hypothalamus—represents solar time to synchronize peripheral tissue clocks in the rest of the body, and drives the expression of daily and seasonal behaviors aligned with the temporal structure of the environment.

Classical behavioral studies performed by manipulating light cycles have revealed fundamental principles in how the brain's circadian clock is reset and synchronized by external time cues at the level of behavioral outputs [1,2]. Entrainment or alignment of circadian locomotive behavior with light cycles is achieved based on differential sensitivity of the circadian rhythm to the timing of light exposure – phase delays in the early circadian night, phase advances in the late night, and a d zone" in the mid-day where light does not reset the rhythm [2]. At the molecular level, the basis of the mammalian circadian clock is self-sustained circadian oscillations of core clock genes arranged in autoregulatory transcription-translation feedback loop (TTFL) where transcription factors CLOCK and BMAL1 drive the circadian expression of *Period* (*Per*) and *Cryptochrome* (*Cry*) genes that mediate negative feedback within the clockworks, through the E-box enhancer elements [3]. Light resetting of the circadian clock is mediated by acute induction of *Per1/2* through the cAMP-response elements (CREs) in the promoter [3]. Transcriptional [4,5] and translational [6] reporters for clock genes have enabled real-time gene expression to assay the motion of the circadian clock. The fundamental question of how core clock genes in the SCN encode different lighting conditions has been primarily addressed by investigating how manipulating light exposure in vivo affects clock gene rhythms subsequently in the SCN explant. This is largely due to technical challenges of mimicking retinal light input in SCN ex vivo, and

imposes interpretational limitations due to the in vivo-ex vivo transition following which the activity of the explanted SCN may not always reflect behavior in vivo [7]. Thus, it remains elusive how exactly the SCN clock alignment with light cycles is achieved in real time over the course of the entrainment at the level of core clock gene rhythms.

Studying circadian entrainment requires long-term periodic stimulation with good temporal precision to repeatedly reset the circadian clockworks – conditions that have been challenging to establish ex vivo. For instance, exogenous application of neurotransmitters involved in light input pathway (e.g., glutamate) lacks the temporal specificity to mimic various types of light cycles. Alternatively, acute optogenetic channelrhodopsin-2 (ChR2) stimulation of SCN neurons with blue light to make them fire at a day-time frequency (as does retinal light input) has high temporal precision, and has been shown to be effective to reset the SCN clock *in vivo* and *ex vivo* [8,9]. However, long-term blue light illumination in culture results in phototoxicity, reducing cell viability [10] and degrading many biological processes, including cell growth [11] and respiration [12]. Notably, cells can tolerate red light better [13,14]. Recent development of optogenetic actuators responding to red light [15,16] prompted us to test whether red light can be utilized for long-term optogenetic stimulation, and address how core clock gene rhythms in the SCN are dynamically altered and reset by repeated stimulation to achieve light entrainment.

We have developed an experimental system integrating red optogenetic stimulation and multi-channel luminometry that enables precise execution of periodic optogenetic stimulation to entrain multiple SCN slices while recording rhythms in the clock gene *Per2* with its bioluminescent translational reporter, PER2::LUC [6]. Using this method, we reveal how the SCN differentially encodes light inputs and light cycles through waveform changes in core clock gene rhythms, and that key aspects of classically described circadian behavioral plasticity are the expression of intrinsic SCN plasticity.

Results

An Integrated System for Long-term Optogenetic Stimulation and Bioluminescence Recording

To entrain the SCN slice with optogenetic stimulation, light pulses must be given periodically for multiple days to weeks. While optogenetically stimulating the SCN with ChR2 has been used to successfully entrain circadian locomotive behavior [8], long-term blue light exposure in culture can decrease cell viability via toxic byproducts [10]. To test the effects of sustained blue light exposure on SCN slices, we delivered blue light pulses (470nm, 10Hz frequency, 10ms width, 1.2mW/mm^2) for 12h to SCN slices expressing a bioluminescent translational reporter of the core clock gene *Per2*, PER2::LUC [6], but no optogenetic construct. We found that PER2::LUC bioluminescence became arrhythmic following the prolonged blue light exposure (Figure 1A and 1B). This effect was not reversible with a medium change (Figure 1A), suggesting that long-term blue light exposure *per se* can elicit photodynamic damage to the SCN slice culture.

Since phototoxicity decreases with increasing irradiation wavelength [14,17], we tested whether using red light (625nm) mitigates the phototoxicity. 12h red light pulses (625nm, 10Hz, 10ms, 1.25mW/mm^2) did not significantly affect the PER2::LUC rhythm in SCN slices (Figure 1A and 1B), suggesting that using red light stimulation is more feasible for prolonged optogenetic light stimulation *ex vivo*. We thus expressed a red light-activated opsin, ChrimsonR [16], in SCN slices using neuron-targeting AAVs (Figure 1C).

To extend the duration over which we can observe the SCN slice throughout entrainment, we improved the quality and robustness of PER2::LUC rhythmicity by using brain slices from younger mice that usually survive longer in culture [18], and by using stabilized glutamine media that helps reduce buildup of toxic ammonia byproduct in culture [19,20] (Figure S1). For precise temporal control of optogenetic stimulation of multiple SCN slices, we integrated an optogenetic

stimulation apparatus into a multi-channel luminometer (Figure 1D). To minimize the potential effect of LED-generated heat on SCN rhythmicity while achieving sufficient light intensity for optogenetic stimulation, we set up a light delivery path in which an LED placed outside the incubator housing the luminometer could deliver 625nm light through a fiber optic cable and a collimation lens (Figure 1D). We then created a program interface for remotely operating PER2::LUC luminometry and optogenetic stimulation in a coordinated manner (Figure S2).

Single Optogenetic Light Pulses Reset SCN Rhythm Phase, Differentially Alter Waveform, and Enduringly Affect Clock Period

To test how this integrated system may induce phase resetting of circadian rhythms that fundamentally underlies circadian entrainment, we applied single optogenetic light stimulations to ChrimsonR-expressing ex vivo SCN slices at three different circadian times (CT) as defined by the timing of the intrinsic PER2::LUC rhythm of each SCN slice. By convention, CT12 was defined as the peak time of the PER2::LUC rhythm and is correlated *in vivo* with the onset of nocturnal behavioral activity [6]. Thus, the rising phase (CT0–12) of the PER2::LUC rhythm represents the day phase of intrinsic SCN circadian time, while the falling phase (CT12–24) corresponds to physiological night. Light stimulation *in vivo* at CT6, CT14, and CT21 induces stereotyped phase responses in the locomotor circadian rhythm (no phase shift, phase delays, and phase advances, respectively) [21,22]. We found that the phase responses to ChrimsonR-mediated stimulation in *ex vivo* SCN indeed mimicked the phase responses of circadian behavior in intact mice to light stimulations *in vivo* (Figure 2A and 2C). Optogenetic stimulation of SCN slices at CT6 induced no phase shifts, whereas optogenetic stimulation at CT14 and CT21 induced phase delays and advances of about 4hr, respectively (Figure 2C).

Strikingly, optogenetic stimulation of SCN slices differentially altered the waveform of PER2::LUC rhythms depending on the timing of the stimulation (Figure 2B). Stimulation at night

(CT14, CT21) induced greater acute increases in PER2::LUC expression in SCN slices than did stimulation in the day (CT6) (Figure 2E). PER2::LUC induction led to changes in the duration of specific phases of PER2::LUC rhythms (Figure 2F). Stimulation at CT14 elongated the falling phase to induce a phase delay, whereas stimulation at CT21 prematurely ended the falling phase and contracted the rising phase to induce a phase advance. Stimulation at CT6, however, did not alter either the rising or the falling phase duration despite a small PER2::LUC induction, thus causing no phase shifts. Together, differential waveform changes in PER2 rhythms mediate time-dependent phase responses to light stimulation in the SCN.

Further, the acute phase shifts were accompanied by a subsequent sustained change in the free-running circadian period (i.e., circadian period of an oscillator in the absence of external time cues such as light) of SCN slices that persisted for multiple days as an after-effect of the acute phase-shifting stimulations (Figure 2A and 2D). Similar to effects on circadian locomotive behavior [1], phase delays in PER2::LUC rhythms led to period lengthening on subsequent cycles, whereas phase advances resulted in period shortening (Figure 2D). Thus, the SCN itself, in isolation from extra-SCN clocks and neural inputs, exhibits plasticity in circadian period following acute light stimulation.

Entrainment of SCN PER2 Rhythms to Different Light-Dark Cycle Lengths Involves Daily Waveform Changes

Individual phase shifts by external time cues are the building blocks of circadian entrainment [2]. Daily, repeated phase shifts to light adjust the endogenous circadian period to match the 24h day and align circadian rhythms in a particular temporal relationship with the daily light-dark cycle (i.e., phase angle of entrainment). To test whether optogenetic stimulation can entrain the isolated SCN clock, we delivered periodic optogenetic light stimulation (optogenetic day-night cycles) with cycle periods that significantly deviated from the near-24h endogenous period of

the SCN (T-cycles), to clearly differentiate the entrained state from free-running. One cohort of SCN slices (T22) was stimulated every 22h while the other cohort (T25) was stimulated every 25h (Figure 3A). SCN in both cohorts demonstrated the classic conditions defining circadian entrainment—matching of clock period to the period of the input stimulus (Figure 3B and S3), adopting a stable timing relationship with the repeating stimulus (stable phase angle, Figure 3C), and initiating a subsequent free-run from the point in time of the entrained phase angle upon cessation of the stimulus (Figure 3A). Importantly, PER2::LUC rhythms in the SCN entrained to the different T-cycles with different phase angles of entrainment (Figure 3C), as predicted by non-parametric model of circadian entrainment, and observed at the level of behavioral outputs [2]. PER2::LUC rhythms under T22 and T25 cycles showed that the periodic stimulation was aligned with the late falling and the late rising phases, where acute stimulation produces a phase advance and a delay, respectively (Figure 3A). Indeed, PER2::LUC rhythms in the SCN were entrained to short and long day-night cycles by daily phase advances and delays, respectively. The daily phase advances and delays were derived from repeated contraction of the PER2::LUC rising phase or elongation of the falling phase, respectively (Figure 3A, 3E, 3F). Taken together, our results demonstrate that PER2::LUC rhythms in SCN slices can entrain to periodic optogenetic stimulation, and reveal that PER2 rhythms in the SCN encode different day-night cycle lengths via repeated rising phase shortening or falling phase lengthening.

We also tested whether PER2 rhythms in SCN slices show plasticity of endogenous clock period in constant darkness following the T-cycle entrainment. T-cycle entrainment by repeated light pulses in vivo produces an after-effect on the period of circadian locomotive behavior: short and long T-cycles produce period shortening and lengthening, respectively [2,23]. As phase shifts by single stimulation had profound period after-effects on PER2::LUC rhythms (Figure 2D), repeated phase shifts by periodic stimulation were expected to have significant period

after-effects. Surprisingly, however, repeated phase advances in PER2::LUC rhythms in SCN slices during T22 entrainment and phase delays during T25 entrainment did not produce statistically significant period after-effects (Figure 3D). This suggests that phase shifts (rather than changes in the endogenous period) are a primary driver of matching circadian PER2 rhythms in the SCN to the period of T-cycles, as proposed by the non-parametric model of entrainment [2].

The SCN Clock Encodes Photoperiods via Differential Changes in PER2 Waveform

Circadian oscillators in the SCN encode the length and timing of the daily light period (i.e., photoperiod) [24,25], thereby promoting seasonal changes in physiology and behavior. Strikingly, light cycles consisting of only brief light pulses defining dawn and dusk (i.e., skeleton photoperiods) have been shown to simulate many aspects of full photoperiods at the behavioral level, with the interval between the brief dawn and dusk pulses determining the photoperiodic state of circadian behavior [2]. This remarkable ability of the circadian system to lock onto the timing of light transitions can, in principle, result from properties of circadian photoreception in the retina (input), downstream behavioral modulation (output), or properties of the SCN clock itself. Here we have tested directly whether the SCN clock itself can be entrained to different photoperiods by brief daily transitions that simulate dawn and dusk.

We applied to SCN slices an optogenetic equivalent of skeleton photoperiods mimicking short (winter-like), equinox, or long (summer-like) photoperiods (8h, 12h, and 16h daylight per day), respectively (Figure 4A and 4B). For the 12:12 skeleton photoperiod entrainment, we gave short optogenetic stimulations (15 min) twice per day (12h apart). We initiated entraining stimulations with one stimulation at the trough of the free-running PER2::LUC rhythm to mimic dawn, and the other stimulation at the peak to mimic dusk (Figure 4A and 4B, 12:12). The 12:12 skeleton indeed entrained SCN slices such that PER2::LUC rhythm period during entrainment became

matched to the 24h optogenetic light cycle length (Figure 4C), and the phase angle of entrainment was stable (measured as the difference in time between the dusk pulse and the half-max on the rising phase of PER2::LUC rhythm, Figure 4D). To test for 8:16 short day skeleton photoperiod entrainment, we initiated twice-daily optogenetic stimulations 8h apart, with the “dawn” pulse given 2h after the trough of the free-running PER2::LUC rhythm, and the “dusk” pulse given 2h before the peak (Figure 4A and 4B, 8:16). The 8:16 skeleton photoperiod entrained PER2::LUC rhythms to 24h period (Figure 4C) with a stable phase angle (Figure 4D) such that the rising phase (SCN day) was encompassed within the 8h “short day” interval between the “dawn” and “dusk” stimulations (Figure 4B). To test for entrainment to 16:8 long day skeleton photoperiods, we initiated optogenetic stimulations twice daily 16h apart, with the “dawn” stimulation applied 2h before the trough and the “dusk” stimulation applied 2h after the peak (Figure 4A and 4B). In contrast to the 12:12 and the 8:16 skeletons, when SCN were presented 16:8 skeleton photoperiods they did not maintain alignment of the PER2::LUC rising phase (SCN day) with the “daytime” interval (16h), but instead rapidly phase-advanced across the “dawn” pulse until achieving similar phase angles to the 8:16 skeleton, stably aligning the SCN day (rising) phase within the 8h short day interval (Figure 4B-4D). Regardless of whether the 8h or 16h interval was first presented aligned with the SCN day phase, isolated SCN always adopted a final phase angle of entrainment consistent with entrainment to a short-day skeleton photoperiod (alignment of the SCN day rising phase within the 8h interval). This phenomenon in the isolated SCN replicates “psi-jumping” of circadian locomotive behavior in rodents [2] (Supplementary Figure 3) and flies [26] during attempted entrainment to long-day skeleton photoperiods, a characteristic expression of circadian plasticity in which entrainment to short-day skeleton photoperiods is more stable. Together, our results indicate that the SCN clock itself can entrain to different photoperiods through the transitions provided by dawn and dusk

light pulses, and suggest that psi-jumping behavior during skeleton photoperiods is derived from SCN-intrinsic clock plasticity.

Entrainment to different skeleton photoperiods also altered the molecular waveform of the SCN clock (Figure 4F). Stimulations at dawn shortened the PER2::LUC rising phase, while stimulations at dusk lengthened the falling phase, to match the clock period to 24h and set the phase angle of entrainment (Figure 4F and 4G). The net effect was that relative duration of the rising phase to the falling phase became shorter than before entrainment in all skeleton photoperiods (Figure 4C). However, changes in the waveform were not sustained in constant darkness after entrainment (Figure 4G), suggesting that the waveform changes are direct effects of optogenetic light stimulation accelerating and decelerating different phases of the molecular clock during entrainment, likely through induction of CRE elements in the *Per2* promoter [3]. Additionally, as a result of entrainment of all SCN in the 8:16 and 16:8 skeleton photoperiods to the 8:16 phase angle, there was a trend toward period lengthening of PER2::LUC rhythms as an after-effect, although these did not reach statistical significance (Figure 4E). This is consistent with previous behavioral studies of period after-effects of skeleton photoperiods [1]. Taken together, skeleton photoperiods entrain PER2 rhythms in the SCN via opposing actions of light pulses on the duration of the rising and the falling phases to match the clock period to 24h.

Discussion

In this study, we assessed dynamics of core clock gene rhythms in the isolated SCN throughout optogenetic stimulation cycles mimicking various types of light entrainment. To accomplish this, we combined bioluminescence recording with red optogenetic stimulation that does not induce

phototoxicity. We have revealed that core clock gene PER2 rhythms in the central clock SCN encode different types of external light cycles via differential changes in duration of specific PER2 phases depending on the timing of light input, and that the SCN clock by itself has the capacity to express light-induced plasticity in entrainment and endogenous period that underlies classically described plasticity in circadian behavior.

Here, we have focused on PER2 as a key clock gene that is rhythmically expressed and light-inducible [3], and identified dynamic landscapes of core clock gene PER2 rhythms that underlie photic effects on circadian rhythms in mammalian locomotive behavior. Acute phase shifts in circadian behavior following a single light pulse are manifested as acute induction of PER2, as seen in vivo [27], and changes in waveform and duration of specific PER2 rhythm phases: phase delays and advances involve elongation of PER2 falling phase and contraction of the rising phase, respectively. The rising and falling phases of the PER2 rhythm represent opposing underlying states of the clockworks: the rising phase represents the synthetic portion of the TTFL where CLOCK and BMAL1 are actively driving transcription, and the falling phase represents the degradative phase in which transcription by CLOCK and BMAL1 is repressed by PERs and CRYs [3]. Our results directly illustrate the acceleration of the rising/synthetic phase by light induction of *Per2* in phase advances, and the prolongation of the falling/degradative phase by *Per2* induction in phase delays. Other core clock gene rhythms (e.g. *Per1*) may have similar landscapes and contribute to remodeling of the clockworks during entrainment.

As daily phase shifts underlie adjustment of the endogenous period of circadian behavior to different day-night cycle lengths, daily waveform changes in specific PER2 phases lead to entrainment of circadian PER2 rhythm to non-24h light cycle periods. Stable alignment of the SCN clock with repeated stimulations at a phase-delaying circadian time achieved circadian entrainment to longer-than-24h cycles via repeated lengthening of the falling phase of PER2,

whereas repeated shortening of the rising phase at a stable phase angle accompanied short T-cycle entrainment. As brief light pulses defining dawn and dusk can entrain circadian behavior, daily light stimulations at dawn and dusk shorten PER2 rising phase and lengthen the falling phase in the SCN, respectively, thereby matching PER2 rhythms to a 24h period.

We have revealed novel insights into intrinsic plasticity of the mammalian central circadian clock. Key principles of circadian entrainment and plasticity in mammals have been discovered by classical behavioral studies that assessed circadian locomotive behavior under different lighting conditions. Circadian behavior, however, is a product of multiple oscillators involving different brain areas, and the SCN receives both extensive feed-forward and feedback from other brain nuclei *in situ* [28]. Our results from ex vivo entrainment of isolated SCN strongly support that many of the classically studied forms of circadian plasticity and properties of entrainment apparently reside intrinsically within the SCN neural network itself. As previously reported [8], the differential phase responses of circadian rhythms depending on the timing of light input is evident even though the SCN neurons are directly stimulated, rather than them receiving retinal input. Furthermore, as entrainment of circadian behavior to different T-cycles is achieved by different phase angles of entrainment, the SCN clock itself establishes different entrained phase angles to T-cycles, consistent with non-parametric model of entrainment [2]. Daily light stimulations fall in the phase-advancing zone (late falling PER2 phase) and the phase-delaying zone (late rising PER2 phase) during short and long T-cycles, respectively. Also, the SCN clock itself can indeed be entrained directly by the light-dark transitions in skeleton photoperiods as mimicked by optogenetic stimulation, and a higher-order aspect of entrainment, such as the bias of the circadian system to resolve ambiguous skeleton light cycles in favor of short-day entrainment [2], also resides in the SCN clockworks.

We uncovered whether and how the SCN clock itself expresses light-induced after-effects in the endogenous clock period. Acute phase shifts produce after-effects on the endogenous period of the SCN clock itself, and interestingly, the magnitude of the period after-effects (up to several hours) is larger than that at the level of behavioral rhythms (up to less than an hour). This suggests that the after-effects on circadian behavior following single light pulse become diminished as light signals are transmitted downstream of the SCN, or that the plasticity of the in vivo SCN is constrained by interactions with extra-SCN oscillators or circuits. In the case of T-cycle entrainment, surprisingly, we did not detect significant period after-effects in the SCN clock, although T-cycle entrainment produces most significant period after-effects in circadian behavior [2]. It is an unexpected finding that repeated stimulation does not produce a large period after-effect, while single light stimulation does. Notably, the clock period of isolated SCN from animals entrained to T-cycles does not represent circadian behavioral period of those animals [29–32], suggesting the possibility that extra-SCN clocks can also influence the behavioral period-aftereffects. Our results from direct entrainment of isolated SCN to T-cycles also suggest that there may be additional clock mechanisms underlying the T-cycle period after-effect beyond our current understanding.

Broadly, our results support a model of SCN entrainment developed from circadian behavioral data in which the SCN clock is predominantly entrained by discrete acute phase shifts to light-dark transitions [2]. While in principle these properties of entrainment and light-history plasticity could arise in vivo from SCN inputs, the SCN itself, or SCN outputs to behavior, our results demonstrate that they are encoded at the molecular level in the SCN itself. Thus, future studies using ex vivo SCN entrainment can further reveal key mechanisms of circadian entrainment and plasticity that underlie alignment of behavioral and physiological rhythms with external time.

Lastly, our system that employs long-term red optogenetic stimulation and bioluminescence recording from cultured neural tissues demonstrates the ability to induce in the isolated SCN neural network the critical process of entrainment, whereby the central clock is synchronized to external time cues. Our method enables *ex vivo* manipulation of the isolated SCN over intervals of days to weeks in a similar way to light entrainment in animals, and evokes plasticity in the SCN clockworks. This system can also be adapted for long-term optogenetic stimulation with other bioluminescent readouts, such as bioluminescence resonance energy transfer (BRET) Ca^{2+} sensors [33,34], and thus it is potentially widely applicable to studying induction of long-term neural plasticity in different regions of the brain.

Method Details

Animals and Housing

P11-14 heterozygous PER2::LUC knock-in mice[6] were used for organotypic slice culture and subsequent procedures. All animals were housed in a 12:12 LD cycle, and had food and water provided ad libitum. Experiments were performed in accordance with the Vanderbilt University Institutional Animal Care and Use Committee and National Institutes of Health guidelines.

Organotypic slice culture and AAV viral transduction

Removed brains were mounted and cut into coronal slices (300μm) on a vibrating blade microtome (Leica) in cold HBSS supplemented with 100 U/ml penicillin/streptomycin, 10 mM HEPES, and 4.5 mM sodium bicarbonate. The SCN slices were dissected out and transferred onto a PTFE membrane insert (Millipore) in 35-mm culture dishes with 1.2 ml of DMEM (D5030, Sigma) supplemented with 3.5 g/L D-glucose, 0.2mM Glutamax (Gibco), 10 mM HEPES, 25 U/ml penicillin/streptomycin, 2% B-27 Plus (Gibco), and 0.1 mM D-Luciferin sodium salt (Tocris).

The SCN slice position was adjusted to the center of the dish and 1.5μl AAV (pAAV1-Syn-ChrimsonR-tdT, Addgene) was placed directly onto the SCN slice. The culture dishes were then sealed with an optically clear PCR plate film (Bio-Rad) and maintained in a non-humidified incubator at 36.8 °C for about 10 days. pAAV1-Syn-ChrimsonR-tdT was a gift from Edward Boyden (Addgene plasmid # 59171)[2]. The opsin expression was checked after about 10 days of viral transduction by imaging tdT fluorescence.

Bioluminescence recording and in situ optogenetic stimulation

After viral transduction, bioluminescence from firefly luciferase in each of PER2::LUC SCN slices was recorded in 6 min intervals by a 32-channel/4-photomultiplier tube luminometer LumiCycle (Actimetrics) in a non-humidified, light-tight incubator at 36.8°C. Baseline rhythms were recorded for at least three days before optogenetic stimulation. For optogenetic stimulation, 625nm LED light (10Hz, 10ms pulse width, 1.5mW/mm^2) was delivered at the center of a target culture dish by a fiber-coupled LED (M625F2, Thorlabs). The LED was located outside the incubator and coupled to a multimode fiber cable (Ø1500μm, 0.39NA) (M93L, Thorlabs) and a fiber collimation package (F230SMA-B, Thorlabs) tethered above samples. Light pulses were generated by an LED driver (LEDD1B, Thorlabs) and a signal generator (Mhinstek). For remotely turning on and off the photomultiplier tubes in the luminometer, a relay switch (Sensata-Crydom) was added in the electrical circuit of the luminometer and connected to a multi-functional I/O device (National Instruments). Custom-written code in Matlab (Mathworks) was used to access luminescence data collection software (Actimetrics), the multi-functional I/O device, and a signal generator software (Mhinstek). The Matlab code loaded a spreadsheet having stimulation settings and time schedules, and executed a series of events during optogenetic stimulation: pause bioluminescence recording, target positioning, stimulation initiation, stimulation termination, and resumption of the recording. For a long light exposure

test, 12h blue or red light pulses (10Hz, 10ms pulse width, 1.2mW/ mm^2) were illuminated onto PER2::LUC SCN slices by LEDs (M470F3 or M625F2, respectively, Thorlabs) coupled to a multimode fiber cable (Ø1500µm, 0.39NA) (M93L, Thorlabs). Blue light-illuminated samples were given a medium change two days after illumination.

Bioluminescence data analysis and visualization

Raw bioluminescence data were baseline-subtracted using 24h running averages and smoothed by 2.4h moving averages using LumiCycle Analysis software (Actimetrics), and then they were loaded as normalized actograms into Matlab-run ClockLab software (Actimetrics) for further analyses. Phase shifts were determined as the time difference between the observed post-stimulation peak of the bioluminescence rhythm and the predicted peak from a linear regression of at least three cycles before stimulation. Period changes were determined as the difference in the period length between the pre-stim and the post-stim cycles. Period length was calculated using a linear regression of at least three peaks. If peaks were not obvious, the period length was determined using half-maxes of the rising phase. For data visualization, smoothed and baseline-subtracted bioluminescence rhythms were represented as double-plotted actograms normalized to min and max values of the data for each line of the actograms, using Excel (Microsoft) and Prism (Graphpad). The actograms were 24h-plotted unless otherwise stated. Bioluminescence rhythms of 12h light-exposed slices were visualized using Excel (Microsoft) and LumiCycle Analysis software (Actimetrics). For quantifying the effect of a long light exposure on the rhythm amplitude, the amplitude of the first post-treatment cycle was normalized to the amplitude of the last pre-treatment cycle. For waveform analyses of single phase shifts, smoothed bioluminescence rhythms with and without stimulation were normalized to extrapolated peak and trough values based on the average dampening rate of the rhythm amplitude over time. Then the rhythms with stimulation were subtracted from those without

stimulation. Normalized induction following stimulation was calculated as the first-cycle amplitude of the subtraction data. For waveform analyses of bioluminescence rhythms during T-cycle entrainment, smoothed bioluminescence rhythms before T22/T25 entrainment and during T22 entrainment were normalized to peak and trough values, and the rhythms during T25 entrainment were normalized to actual troughs and interpolated peaks based on the first cycle of the free-running rhythms released in constant darkness. For waveform analyses of bioluminescence rhythms during skeleton photoperiods, the smoothed first derivatives were taken from the smoothed, baseline-subtracted bioluminescence rhythms normalized to min and max values, using Excel (Microsoft) and Prism (Graphpad). The duration of the rising and falling phases was determined using the time duration between the zero crossings of the first derivatives. If the first derivatives were close to zero but did not make a zero crossing due to an increase immediately following an optogenetic stimulation, the local minimum was defined as the end of the rising phase. Waveform data were visualized using Excel (Microsoft) and Prism (Graphpad).

Statistical analysis

All statistical analyses (Student's t-test, Ratio paired t-test, One-Way ANOVA with Tukey's multiple comparisons tests, RM Two-way ANOVA with Sidak's multiple comparisons tests) were performed in Prism (Graphpad). Data are presented as a mean ± standard error of mean (SEM) and differences between groups were considered statistically significant when $p < 0.05$.

Acknowledgments:

We would like to thank Michael Hastings for help in improving our SCN culture medium. This study was supported by Vanderbilt International Scholarship to S.K. and NIH R01 GM117650 to D.G.M.

Author Contributions:

S.K. and D.G.M. conceived of the project. S.K performed all the experiments. S.K and D.G.M. wrote the manuscript.

References

1. Pittendrigh, C.S., and Daan, S. (1976). A functional analysis of circadian pacemakers in nocturnal rodents - I. The stability and lability of spontaneous frequency. J. Comp. Physiol. *106*, 223–252.

2. Pittendrigh, C.S., and Daan, S. (1976). A functional analysis of circadian pacemakers in nocturnal rodents - IV. Entrainment: Pacemaker as clock. J. Comp. Physiol. *106*, 291–331.

3. Takahashi, J.S. (2017). Transcriptional architecture of the mammalian circadian clock. Nat. Rev. Genet. *18*, 164–179.

4. Yamaguchi, S., Mitsui, S., Miyake, S., Yan, L., Onishi, H., Yagita, K., Suzuki, M., Shibata, S., Kobayashi, M., and Okamura, H. (2000). The 5' upstream region of mPer1 gene contains two promoters and is responsible for circadian oscillation. Curr. Biol. *10*, 873–876.

5. Kuhlman, S.J., Quintero, J.E., and McMahon, D.G. (2000). GFP fluorescence reports Period1 circadian gene regulation in the mammalian biological clock. Neuroreport *11*, 1479–1482.

6. Yoo, S.H., Yamazaki, S., Lowrey, P.L., Shimomura, K., Ko, C.H., Buhr, E.D., Siepka, S.M., Hong, H.K., Oh, W.J., Yoo, O.J., *et al.* (2004). PERIOD2::LUCIFERASE real-time reporting of circadian dynamics reveals persistent circadian oscillations in mouse peripheral tissues. Proc. Natl. Acad. Sci. U. S. A. *101*, 5339–5346.

7. Pendergast, J.S., Friday, R.C., and Yamazaki, S. (2009). Endogenous rhythms in period1 mutant suprachiasmatic nuclei in vitro do not represent circadian behavior. J. Neurosci. *29*, 14681–14686.

8. Jones, J.R., Tackenberg, M.C., and McMahon, D.G. (2015). Manipulating circadian clock neuron firing rate resets molecular circadian rhythms and behavior. Nat. Neurosci. *18*, 1–5.

9. Mazuski, C., Abel, J.H., Chen, S.P., Hermanstyne, T.O., Jones, J.R., Simon, T., Doyle, F.J., and Herzog, E.D. (2018). Entrainment of Circadian Rhythms Depends on Firing Rates and Neuropeptide Release of VIP SCN Neurons. Neuron *99*, 555-563.e5.

10. Stockley, J.H., Evans, K., Matthey, M., Volbracht, K., Agathou, S., Mukanowa, J., Burrone, J., and Káradóttir, R.T. (2017). Surpassing light-induced cell damage in vitro with novel cell culture media. Sci. Rep. *7*, 1–11.

11. Ohara, M., Kawashima, Y., Katoh, O., and Watanabe, H. (2002). Blue light inhibits the growth of B16 melanoma cells. Japanese J. Cancer Res. *93*, 551–558.

12. Robertson, J.B., Davis, C.R., and Johnson, C.H. (2013). Visible light alters yeast metabolic rhythms by inhibiting respiration. Proc. Natl. Acad. Sci. U. S. A. *110*, 21130–21135.

13. Godley, B.F., Shamsi, F.A., Liang, F.Q., Jarrett, S.G., Davies, S., and Boulton, M. (2005). Blue light induces mitochondrial DNA damage and free radical production in epithelial cells. J. Biol. Chem. *280*, 21061–21066.

14. Waldchen, S., Lehmann, J., Klein, T., Van De Linde, S., and Sauer, M. (2015). Light-induced cell damage in live-cell super-resolution microscopy. Sci. Rep. *5*, 1–12.

15. Lin, J.Y., Knutsen, P.M., Muller, A., Kleinfeld, D., and Tsien, R.Y. (2013). ReaChR: A red-shifted variant of channelrhodopsin enables deep transcranial optogenetic excitation. Nat. Neurosci. *16*, 1499–1508.

16. Klapoetke, N.C., Murata, Y., Kim, S.S., Pulver, S.R., Birdsey-Benson, A., Cho, Y.K.,

Morimoto, T.K., Chuong, A.S., Carpenter, E.J., Tian, Z., *et al.* (2014). Independent optical excitation of distinct neural populations. Nat. Methods *11*, 338–346.

17. Tyssowski, K.M., and Gray, J.M. (2019). Blue light increases neuronal activity-regulated gene expression in the absence of optogenetic proteins. eNeuro *6*, 0085–19.2019.

18. Humpel, C. (2015). Neuroscience forefront review organotypic brain slice cultures: A review. Neuroscience *305*, 86–98.

19. Christie, A., and Butler, M. (1999). The adaptation of bhk cells to a non-ammoniagenic glutamate-based culture medium. Biotechnol. Bioeng. *64*, 298–309.

20. Imamoto, Y., Tanaka, H., Takahashi, K., Konno, Y., and Suzawa, T. (2013). Advantages of AlaGln as an additive to cell culture medium: Use with anti-CD20 chimeric antibody-producing POTELLIGENT^{TM} CHO cell lines. Cytotechnology *65*, 135–143.

21. Daan, S., and Pittendrigh, C.S. (1976). A Functional analysis of circadian pacemakers in nocturnal rodents - II. The variability of phase response curves. J. Comp. Physiol. *106*, 253–266.

22. Johnson, C.H. (1999). Forty years of PRCs - What have we learned? Chronobiol. Int. *16*, 711–743.

23. Schwartz, W.J., Tavakoli-Nezhad, M., Lambert, C.M., Weaver, D.R., and De La Iglesia, H.O. (2011). Distinct patterns of Period gene expression in the suprachiasmatic nucleus underlie circadian clock photoentrainment by advances or delays. Proc. Natl. Acad. Sci. U. S. A. *108*, 17219–17224.

24. Rusak, B., and Morin, L.P. (1976). Testicular Responses to Photoperiod Are Blocked by Lesions of the Suprachiasmatic Nuclei in Golden Hamsters1. Biol. Reprod. *15*, 366–374.

25. Goldman, B.D. (2001). Mammalian Photoperiodic System: Formal Properties and Neuroendocrine Mechanisms of Photoperiodic Time Measurement. J. Biol. Rhythms *16*, 283–301.

26. Pittendrigh, C.S., and Minis, D.H. (1964). The Entrainment of Circadian Oscillations by Light and Their Role as Photoperiodic Clocks. Am. Nat. *98*, 261–294.

27. Yan, L., and Silver, R. (2002). Differential induction and localization of mPer1 and mPer2 during advancing and delaying phase shifts. Eur. J. Neurosci. *16*, 1531–1540.

28. Dibner, C., Schibler, U., and Albrecht, U. (2010). The Mammalian Circadian Timing System: Organization and Coordination of Central and Peripheral Clocks. Annu. Rev. Physiol. *72*, 517–549.

29. Aton, S.J., Block, G.D., Tei, H., Yamazaki, S., and Herzog, E.D. (2004). Plasticity of circadian behavior and the suprachiasmatic nucleus following exposure to non-24-hour light cycles. J. Biol. Rhythms *19*, 198–207.

30. Azzi, A., Evans, J.A., Leise, T., Myung, J., Takumi, T., Davidson, A.J., and Brown, S.A. (2017). Network Dynamics Mediate Circadian Clock Plasticity. Neuron *93*, 441–450.

31. Ciarleglio, C.M., Resuehr, H.E.S., Axley, J.C., Deneris, E.S., and McMahon, D.G. (2014). Pet-1 Deficiency Alters the Circadian Clock and Its Temporal Organization of Behavior. PLoS One *9*, e97412.

32. Molyneux, P.C., Dahlgren, M.K., and Harrington, M.E. (2008). Circadian entrainment aftereffects in suprachiasmatic nuclei and peripheral tissues in vitro. Brain Res. *1228*, 127–134.

33. Yang, J., Cumberbatch, D., Centanni, S., Shi, S.Q., Winder, D., Webb, D., and Johnson, C.H. (2016). Coupling optogenetic stimulation with NanoLuc-based luminescence (BRET)

Ca++ sensing. Nat. Commun. *7*, 13268.

34. Suzuki, K., Kimura, T., Shinoda, H., Bai, G., Daniels, M.J., Arai, Y., Nakano, M., and Nagai, T. (2016). Five colour variants of bright luminescent protein for real-time multicolour bioimaging. Nat. Commun. *7*, 13718.

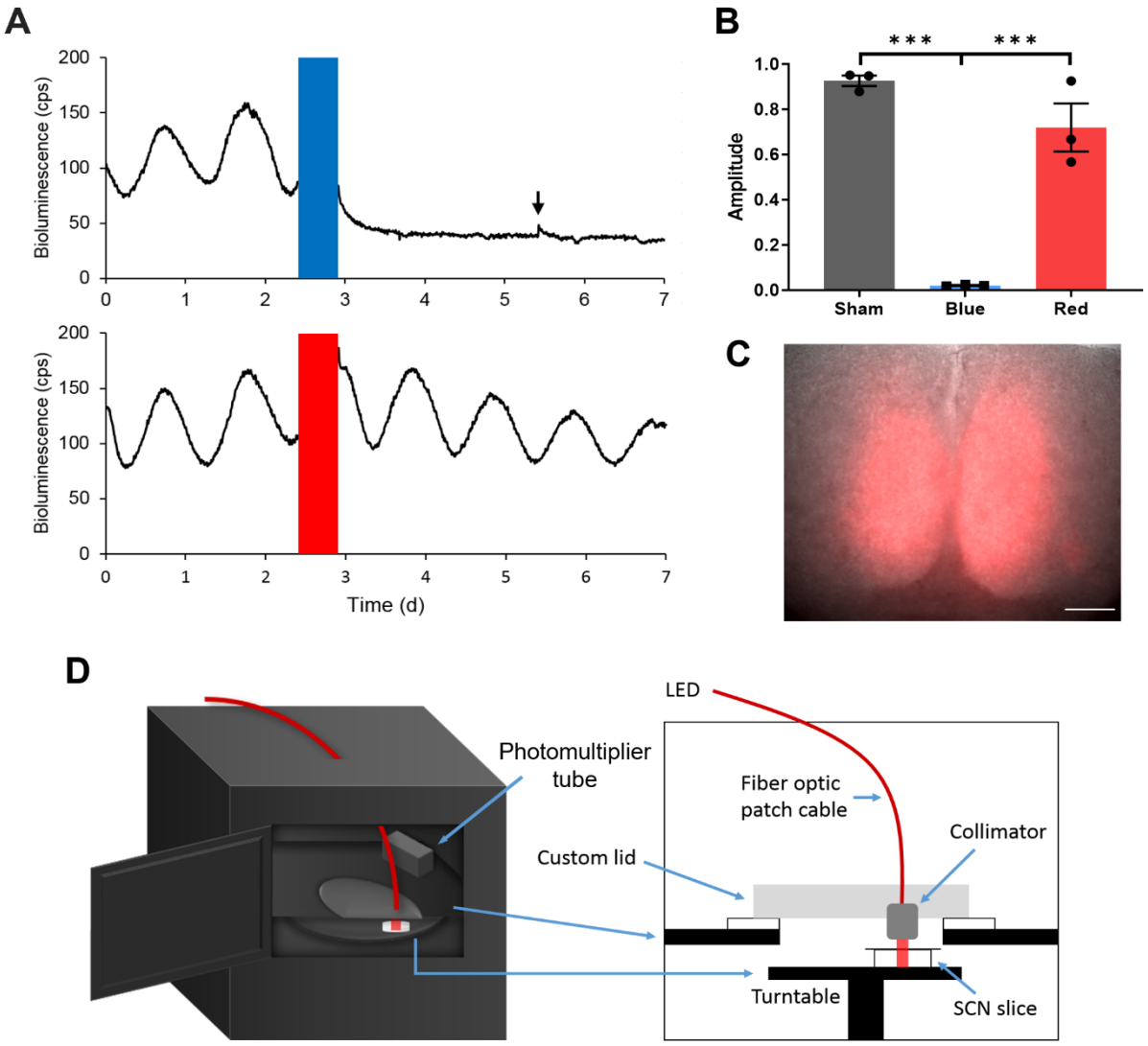
A
Bioluminescence (cps)
200
150
100
50
0
0 1 2 3 4 5 6 7
Time (d)
B
***
***
Amplitude
1.0
0.8
0.6
0.4
0.2
0.0
Sham
Blue
Red
C
D
LED
Photomultiplier tube
Fiber optic patch cable
Collimator
Custom lid
Turntable
SCN slice

Figure 1. Long-term Optogenetic Stimulation System for Circadian Entrainment Ex Vivo.
(A) Representative PER2::LUC bioluminescence rhythms of SCN slices exposed to either red (top) or blue (bottom) 10Hz light pulses (red or blue bars) for 12h. The black arrow indicates the timing of media change.
(B) Fold change in the rhythm amplitude following sham, blue, or red light exposure (Student t-test, mean ± SEM, n = 3, ***$p < 0.001$).
(C) Merged ChrimsonR-tdT fluorescence and the brightfield images of an SCN slice. Scale = 100μm.
(D) Diagrams showing a multi-channel luminometer integrated with an optogenetic stimulation apparatus.

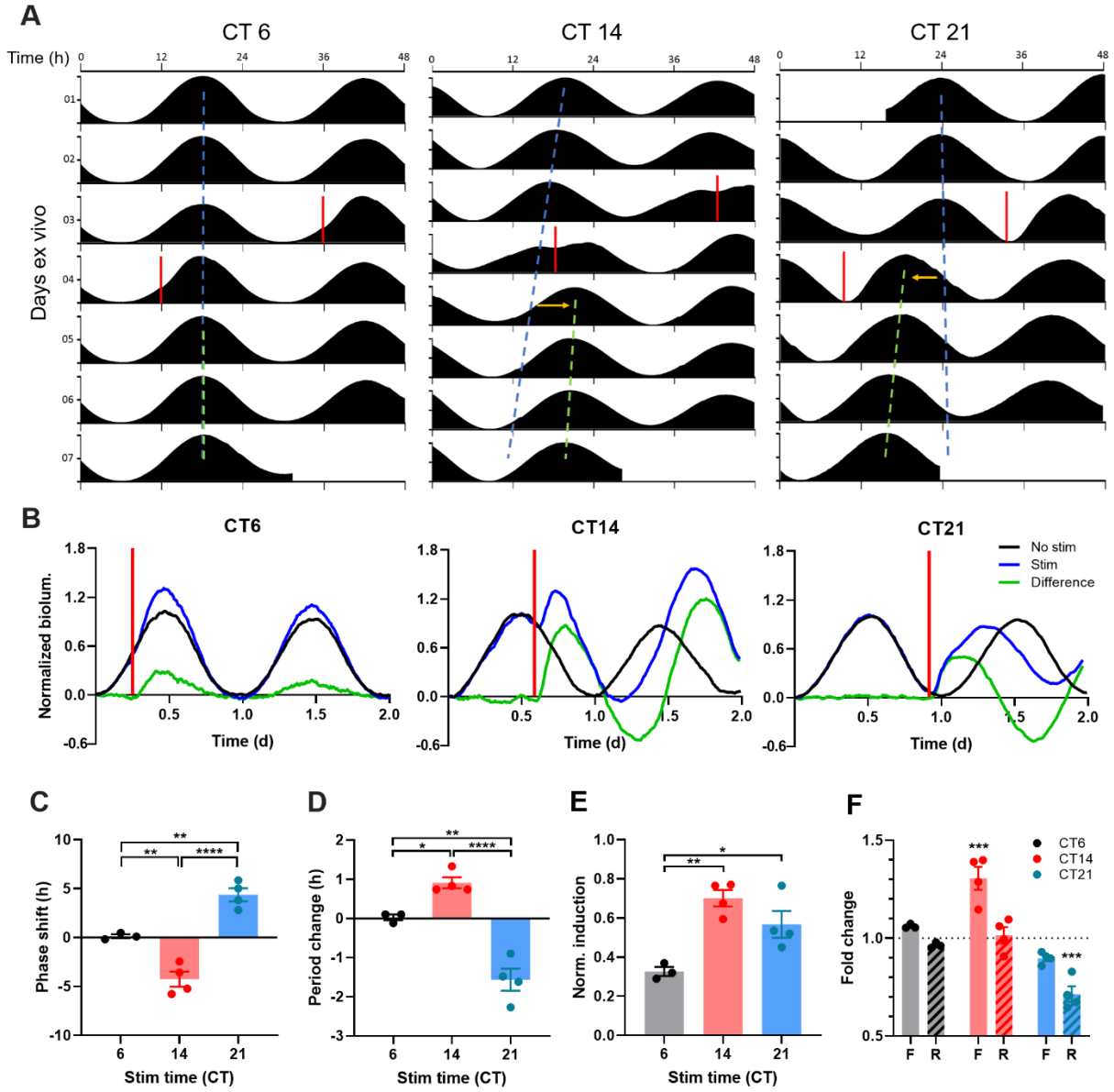
A
CT 6
CT 14
CT 21
Time (h)
Days ex vivo
B
CT6
CT14
CT21
Normalized biolum.
Time (d)
No stim
Stim
Difference
C
Phase shift (h)
Stim time (CT)
D
Period change (h)
Stim time (CT)
E
Norm. induction
Stim time (CT)
F
Fold change
CT6
CT14
CT21

Figure 2. ChrimsonR-driven Optogenetic Stimulation Alters the Waveform of SCN PER2 Rhythm to Reset the SCN Clock.

(A) Representative double-plotted PER2::LUC bioluminescence actograms of SCN slices stimulated with single 15min 10Hz optogenetic pulses (red bar) at CT6 (left), 14 (middle), and 21 (right). Linear regressions of the pre-stimulation and post-stimulation cycle peaks are indicated as the blue and green dashed lines, respectively. Phase shifts are depicted by a yellow arrow.

(B) Representative PER2::LUC rhythms of SCN slices before and after stimulation (red bar). Green traces depict difference in normalized bioluminescence between the pre-stim and post-stim rhythms (black and blue traces, respectively).

(C and D) Quantification of phase shifts (C) and period changes (D) following stimulation. Positive and negative phase shifts indicate phase advance and delay, respectively. Positive and negative period changes indicate period lengthening and shortening, respectively. (One-way ANOVA with Turkey's multiple comparisons test, mean ± SEM, n = 3-4, *$p < 0.05$, **$p < 0.01$).

(E) Normalized PER2::LUC induction following stimulation. (One-way ANOVA with Turkey's multiple comparisons test, mean ± SEM, n = 3-4, *$p < 0.05$, **$p < 0.01$).

(F) Fold change in duration of the rising and falling phases of PER2::LUC rhythms following stimulation. (RM two-way ANOVA with Sidak's multiple comparisons tests, mean ± SEM, n = 3-4, ***$p < 0.001$).

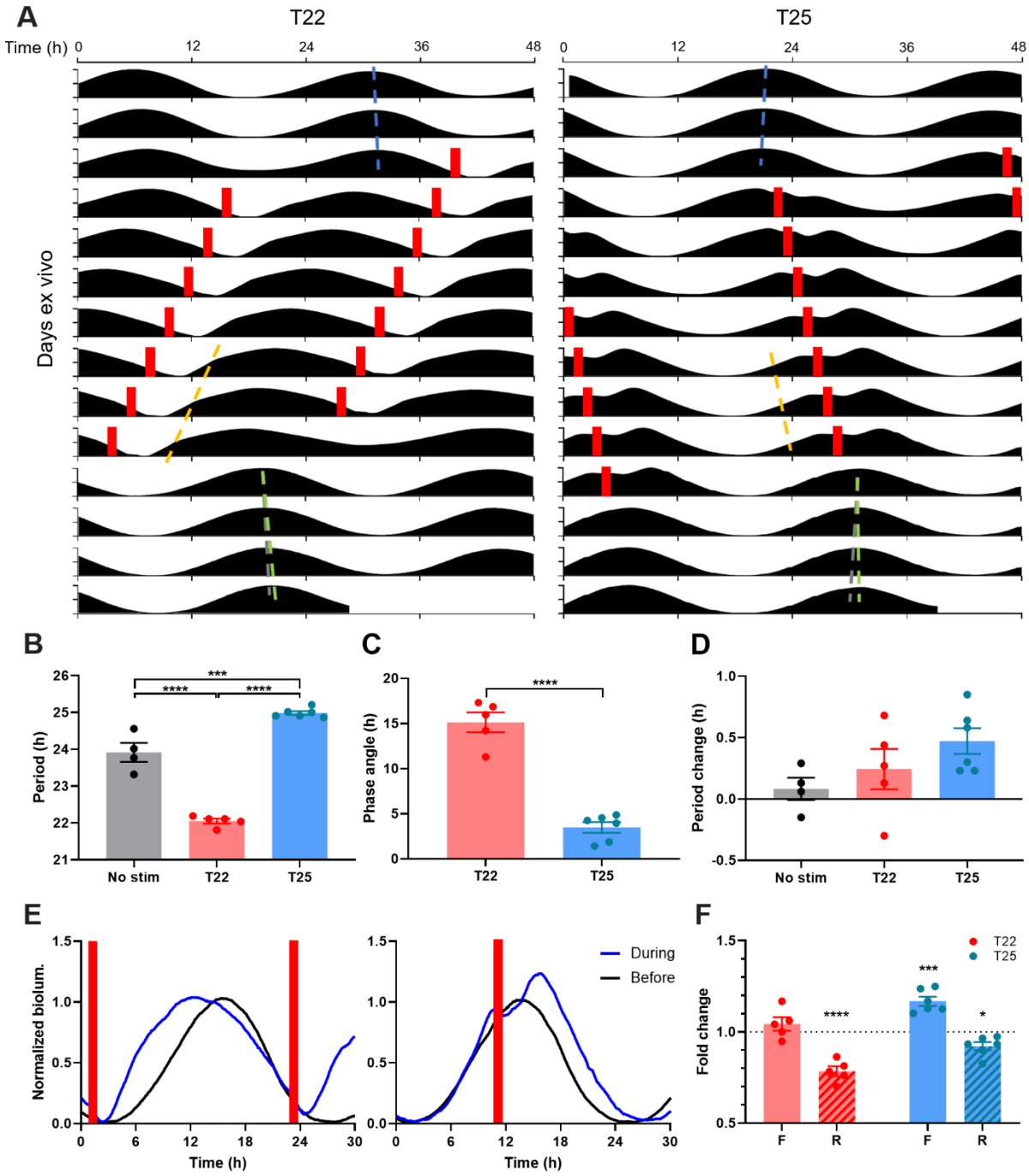
A
T22
T25
Time (h)
Days ex vivo
B
Period (h)
No stim
T22
T25
C
Phase angle (h)
D
Period change (h)
E
Normalized biolum.
Time (h)
During
Before
F
Fold change
F
R

Figure 3. Optogenetic T-cycles Entrain PER2::LUC Rhythms in the SCN by Triggering Daily Waveform Changes that Match the SCN Clock to the T-cycle Period.
(A) Representative double-plotted PER2::LUC bioluminescence actograms of the SCN slice entrained with 1–1.5h 10Hz optogenetic pulse (red bar) in every 22h (left) or 25h (right). Linear regressions of the pre- and post-entrainment cycle peaks are indicated as the blue and green dashed lines, respectively. Yellow dashed lines indicate half-maxes on the rising phase during entrainment. Grey dashed lines indicate the pre-entrainment cycle period as a reference.
(B-D) Quantification of period during entrainment (B), phase angle of entrainment (C), period change by entrainment (D). (B and D) were analyzed using one-way ANOVA with Turkey's multiple comparisons tests (mean ± SEM, n = 4-6, ****$p < 0.0001$, ***$p < 0.001$), (C) was analyzed using Student t-test (mean ± SEM, n = 5-6, ****$p < 0.0001$).
(E) Representative waveforms of PER2::LUC bioluminescence rhythms before (black trace) and during (blue trace) entrainment to T22 (left) and T25 cycles (right). Red bars depict optogenetic stimulation during entrainment.
(F) Fold change in duration of the rising and falling phases of PER2::LUC rhythms during entrainment compared with before entrainment. (RM two-way ANOVA with Sidak's multiple comparisons tests, mean ± SEM, n = 5-6, ***$p < 0.001$, ****$p < 0.0001$).

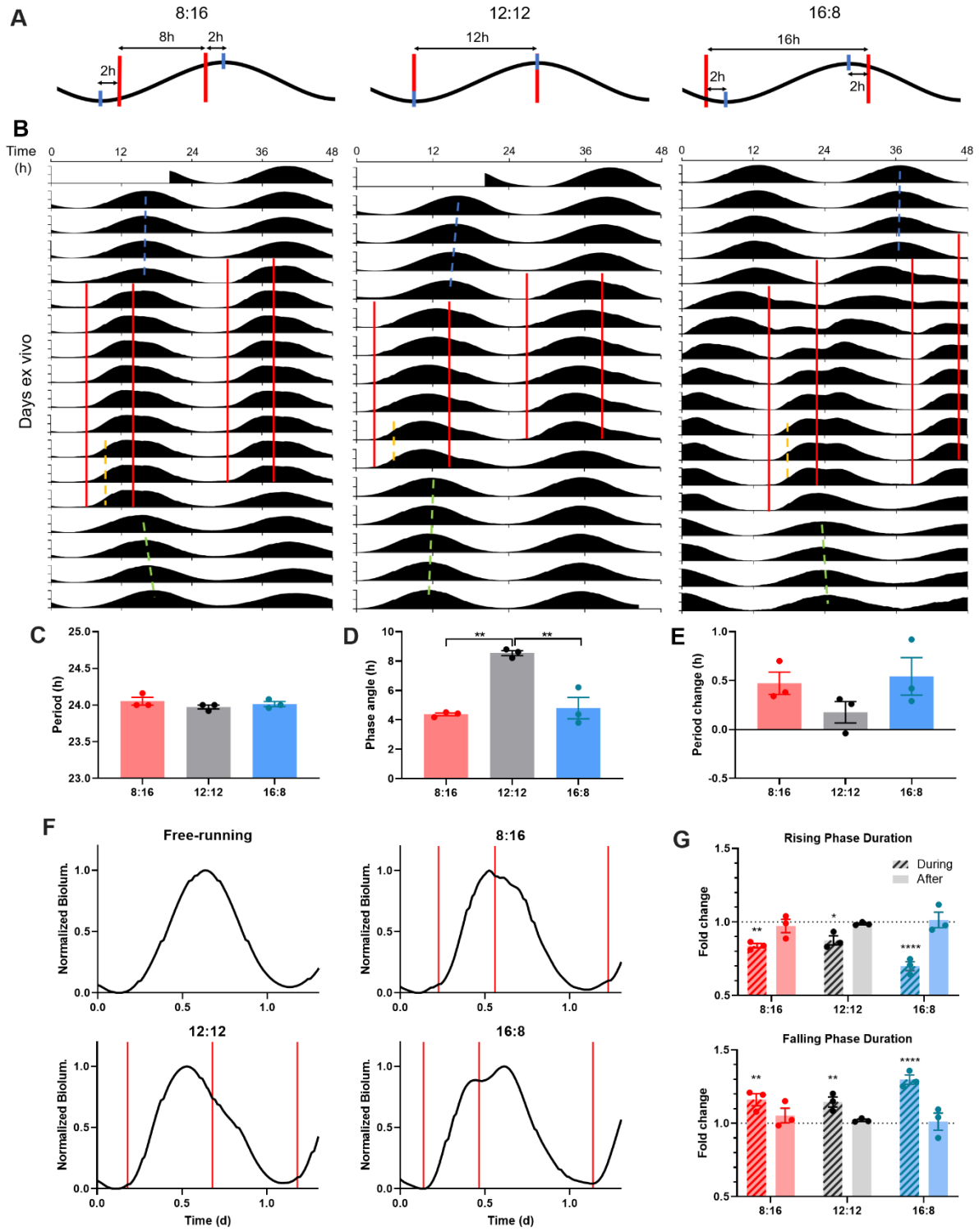
A
8:16
8h
2h
2h
12:12
12h
16:8
16h
2h
2h
B
Time (h)
0
12
24
36
48
Days ex vivo
C
Period (h)
25.0
24.5
24.0
23.5
23.0
8:16
12:12
16:8
D
Phase angle (h)
10
8
6
4
2
0
**
**
8:16
12:12
16:8
E
Period change (h)
1.0
0.5
0.0
-0.5
8:16
12:12
16:8
F
Free-running
8:16
12:12
16:8
Normalized Biolum.
1.0
0.5
0.0
0.0
0.5
1.0
Time (d)
G
Rising Phase Duration
During
After
Fold change
1.5
1.0
0.5
**
*
****
8:16
12:12
16:8
Falling Phase Duration
Fold change
1.5
1.0
0.5
**
**
****
8:16
12:12
16:8

Figure 4. PER2::LUC Rhythms in the SCN Entrain to Optogenetic Skeleton Photoperiods via Differential Changes in Duration of Specific Phases

(A) Schematic diagram of optogenetic stimulation paradigm for 8:16 (left), 12:12 (middle), and 16:8 (right) skeleton photoperiod entrainment. Optogenetic pulses (red bars) were given twice (8h, 12h, or 16h apart) every 24h, targeting near the peak and trough (blue ticks) of PER2::LUC rhythms (black).

(B) Representative double-plotted PER2::LUC bioluminescence actograms of SCN slices entrained with 15-min 10Hz red optogenetic pulses (red bars) at 8:16 (left), 12:12 (middle), or 16:8 (right) interval of 24h. Linear regressions of the pre-, post-entrainment cycle peaks and during-entrainment cycle half-maxes are indicated as the blue, green, and yellow dashed lines, respectively.

(C-E) Quantification of period during entrainment (C), phase angle of entrainment (D), period change following entrainment (E). (One-way ANOVA with Turkey's multiple comparisons test, mean ± SEM, n = 3, **$p < 0.01$).

(F) Representative waveforms of PER2::LUC rhythms in SCN slices in a free-running condition (before and after entrainment), and those entrained to optogenetic 8:16, 12:12, 16:8 photoperiod entrainment. Optogenetic light pulses were given at times indicated by red lines.

(G) Fold changes in the peak of the rising phase slope (G) and in the relative duration of the rising phase to the falling phase (H) during and after entrainment, compared to before entrainment. (RM two-way ANOVA with Dunnett's multiple comparisons tests, mean ± SEM, n = 3, *$p < 0.05$, **$p < 0.01$, ****$p < 0.0001$).